Article

Not peer-reviewed version

# Relationship between CT Derived Bone Mineral Density and UTE-MR Derived Porosity Index in Equine Third Metacarpal and Metatarsal Bones

Carola Daniel *, Sarah Elizabeth Taylor *, Sam McPhee, Uwe Wolfram, Tobias Schwarz, Stefan Sommer, Lucy Kershaw

Posted Date: 7 August 2023

doi: 10.20944/preprints202308.0477.v1

Keywords: bone mineral density; porosity index; MRI; ultra-short echo time; CT; equine; lateral condylar fracture; palmar osteochondral disease; stress fracture; fatigue injury

*Article*

# Relationship between CT Derived Bone Mineral Density and UTE-MR Derived Porosity Index in Equine Third Metacarpal and Metatarsal Bones

**CR Daniel [1,*,†], SE Taylor [1,*,†], S McPhee [2], U Wolfram [2], T Schwarz [1], S Sommer [3,4,5] and LE Kershaw [6]**

[1] Royal (Dick) School of Veterinary Studies and The Roslin Institute, The University of Edinburgh, Edinburgh, United Kingdom
[2] Institute of Mechanical, Process and Energy Engineering, School of Engineering and Physical Sciences, Heriot- Watt University, Edinburgh, United Kingdom
[3] Siemens Healthcare, Zurich, Switzerland
[4] Swiss Center for Musculoskeletal Imaging (SCMI), Balgrist Campus, Zurich, Switzerland
[5] Advanced Clinical Imaging Technology (ACIT), Siemens Healthcare AG, Lausanne, Switzerland
[6] Centre for Cardiovascular sciences and Edinburgh Imaging, The University of Edinburgh, Edinburgh, United Kingdom
* Correspondence: to whom correspondence should be addressed.
† These authors contributed equally to this work.

**Simple Summary:** Racehorses have similar health issues to human runners during their career. The intense exercise regime leads to changes in their bone composition; the bones become more dense and less porous to adapt to the higher than usual demands. While this is generally beneficial, the bone also becomes more brittle in the process, which can result in stress fractures in human athletes and racehorses alike. The balance between beneficial training responses and overtraining is fine and we are currently not able to use imaging techniques to distinguish reliably between the two of them, before injury occurs. Two important markers of bone health are the density of bone, which is well established, and the number of pores within the bone tissue, which has recently become of more interest. We aim to validate a new MRI-based technique to measure bone porosity in horses. This has the potential to improve our understanding of bony changes associated with training in racehorses and aid identification of factors associated with fracture risk.

**Abstract:** Fatigue-related subchondral bone injury of the third metacarpal/ metatarsal (McIII/ MtIII) bone is a common cause of wastage and welfare concern in racehorses. Better understanding of bone health and strength would improve animal welfare and be of benefit for the racing industry. Porosity index (PI) of bone is an indirect measure of osseous pore size and number and is therefore an interesting indicator of bone strength. MRI of compact bone using traditional methods even with short echo times fails to generate enough signal to assess bone architecture as the water protons are tightly bound. Ultrashort echo time (UTE) sequences aim to increase the amount of signal detected in the equine McIII/MtIII condyle. Cadaver specimens were imaged using a novel dual-echo UTE MRI technique and PI was calculated and validated against quantitative CT-derived bone mineral density (BMD). BMD and PI are inversely correlated in the equine distal Mc/ MtIII with a mean r value of -0.29. The r value is significantly different between fore- and hindlimbs. Further work is needed to assess how correlation patterns behave in different areas of the bone and to evaluate PI in horses with and without clinically relevant stress injury.

**Keywords:** bone mineral density; porosity index; MRI; ultra-short echo time; CT; equine; lateral condylar fracture; palmar osteochondral disease; stress fracture; fatigue injury

 doi:10.20944/preprints202308.0477.v1



## 1. Introduction

Racehorses experience high volumes of intense exercise, resulting in increased cyclic loading of their musculoskeletal system and increased risk of stress injury. The most commonly reported fatigue injuries in racehorses are palmar/ plantar osteochondral disease (POD) [1] and fractures of the third metacarpal and metatarsal bones (McIII and MtIII) [2].

POD is a common condition affecting the subchondral bone of the palmar and plantar distal condyles of McIII and MtIII. The condition is usually most pronounced in the thoracic limbs at the medial condyles, however the pelvic limbs can also be affected where the lateral condyles are predominantly diseased [3]. In addition to subchondral bone lesions, cartilage ulceration and wear lines can be found in affected horses [1]. Lesion severity ranges from discoloration of the subchondral bone to disruption of the osseous and cartilaginous surface, creating a full thickness focal defect [1,4]. Pain associated with subchondral bone injury is well documented and associated with performance limiting lameness in the equine patient [5]. Radiographic assessment of POD lesions shows low sensitivity and specificity but can be aided by secondary features of advanced disease such as osteophytes on the proximal sesamoid bones, cavitation of dorso-distal aspect of McIII or flattening of the palmar consyles [6]. *In vivo* standing low field MRI is able to identify osseous changes associated with palmar osteochondral disease prior to radiographic changes [7] and high field MRI can assess cartilaginous involvement [8], but *in vivo* differentiation of physiological rather than pathological subchondral bone pathology as seen in the early stages of the disease, remains difficult. To avoid progression of disease to debilitating stages, early detection would be beneficial. Furthermore, in some cases, stress induced subchondral bone injury has the potential to propagate into potentially catastrophic fractures [9,10].

Fractures of McIII and MtIII are common injuries in racehorses and are associated with animal welfare concerns [11,12] and financial loss [13]. The most common fracture site is the lateral condyle of McIII or MtIII emanating from or near the parasagittal groove [2,12]. These fractures are classified as fatigue fractures [14] and represent a known clinical problem in human and equine athletes alike [15,16]. In these patient groups repetitive excessive strain from high volume training leads to accumulation of microtrauma, which over time reduces bone stiffness and decreases bone strength [17,18]. Eventually the accumulation of microdamage is greater than the reparative capacity of the osseous tissue and catastrophic fractures can occur. While assessment of accumulative osseous microdamage represents an interesting tool to investigate fracture risk, it is currently limited to experimental *ex vivo* imaging as suitable *in vivo* imaging modalities are missing [16,19]. Furthermore, commercially available microCT scanners only allow imaging of small samples due to size restrictions, assessment of a whole bone as an uninterrupted anatomical and biomechanical unit is unattainable.

Bone mineral density (BMD) is widely used in human medicine as an indirect measure of fracture risk, particularly in osteoporosis [20]. While traditionally measured via dual-energy X-ray absorptiometry (DEXA), the use of quantitative computed tomography (QCT) has recently come to the forefront [21]. In the equine patient QCT has shown greater BMD values in response to race training in the diaphyseal and condylar portion of McIII, however no significant difference between fracture patients and controls could be identified in two studies [22,23]. However, the results of work by Loughridge et al. (2017) were at variance with previous studies showing a significantly higher bone density in fractured McIII when compared to controls [24]. The use of QCT derived BMD measurements remains of interest in a clinical context, as it allows the use of whole, undissected specimens as well as *in vivo* data derived from clinical patients.

In addition to the mineral component, the porosity of cortical and trabecular bone plays a major role in bone strength and stifness [25,26] and has been associated with fractures independent of bone density [27,28]. While traditionally bone and bone porosity were assessed with radiation-based modalities, MRI has recently enjoyed increasing popularity. Ultra short echo time (UTE) MRI is a novel technique capable of imaging cortical bone. While in conventional MR sequences the signal decay times of cortical bone are too short to generate detectable signal, the echo times in UTE sequences allow sufficient signal detection to image the cortical bone even with its tightly bound

 doi:10.20944/preprints202308.0477.v1



water protons. Whereas previous efforts have focussed on simply reducing echo time (TE) in bone imaging, recently the focus has shifted towards differentiating between the two pools of labile water protons: bound water (BW) and pore water (PW) [29]. Water, which can move freely within the osseous pores (= PW) has a longer T2* relaxation time than collagen-bound water (BW). Signal derived from PW is an indirect measure of the amount of pore space within cortical bone and has been shown to be indirectly proportional to bending strength, as well as agreeing with microCT-derived porosity [30,31]. Porosity index (PI) is defined as the ratio between PW and BW and can be computed by using a dual-echo technique, acquiring PW as well as BW images. For this technique two images are acquired, one with a relatively long echo time, which solely contains signal from PW, as the BW signal has fully decayed at read out. The other image uses a relatively short echo time and will therefore include signal from both water proton pools. Dividing the long echo time image by the short echo time image will result in a PI image [30,32]. A strong correlation between microCT-derived porosity index, pore size and bone stiffness has been described in *ex vivo* experiments and human patients [30,32,33].

We aimed to validate the use of a dual-echo UTE research application sequence for the measurement of PI in the equine patient against a peripheral quantitative CT (QCT). Furthermore, we hypothesised that BMD and PI are inversely correlated in the in the distal McIII/ MtIII of racehorses in training, in keeping with data known from human patients. We further aim to investigate potential differences between forelimbs and hindlimbs and the left and right side. PI could serve as an indicator of bone health and strength and aid our understanding of pathophysiological processes in the context of osseous stress remodelling and fatigue injury in the equine athlete.

## 2. Materials and Methods

### *Animals*

Specimens were derived from six Thoroughbred racehorses in training (age: 3 to 9 years, 2 mares, 4 geldings). All animals were subjected to euthanasia between November 2021 and April 2022 for non-study related reasons and their limbs donated to research (VERC 165.22). Twelve forelimbs and twelve hindlimbs were harvested within 24 hours after the death of the animal. Specimens were disarticulated in the carpal and tarsal joints respectively and frozen at -20° for various time periods until further processing.

### *CT imaging*

All specimens underwent high-resolution peripheral quantitative computed tomography in a 64-slice CT scanner (Somatom Definition AS, Siemens Healthcare, Erlangen, Germany; voltage: 120 kV, current: 80 mA, matrix size: 512 x 512, slice thickness: 0.6 mm, voxel size of 0.273 mm x 0.273 mm x 0.4 mm). Limbs were scanned with a standard clinical hydroxyapatite phantom (model number 8783219, Siemens, Germany) to allow calibration to a bone mineral density scale.

### *MR imaging*

All specimens were brought to room temperature over 24 hours prior to MR imaging. Dual-echo UTE images were acquired using a 3T clinical scanner (MAGNETOM Skyra 3T, Siemens Healthcare, Erlangen, Germany; $TE_{short}$: 0.04ms, $TE_{long}$: 2.52ms, TR: 12 ms 5, average voxel size: 0.3mm$^3$).

### *Image processing*

The raw 16-bit grey-level QCT images were parsed to a BMD scale by linear transformation based on the hydroxyapatite/ demineralized water phantom using ImageJ (NIH Image J 1.53) [34,35]. PI images were generated by dividing the echo intensity images acquired with $TE_{long}$ by the echo intensity of images acquired with $TE_{short}$ and multiplying the result by 100% (see Figure 1) using python.

Preprints (www.preprints.org) | NOT PEER-REVIEWED | Posted: 7 August 2023 doi:10.20944/preprints202308.0477.v1



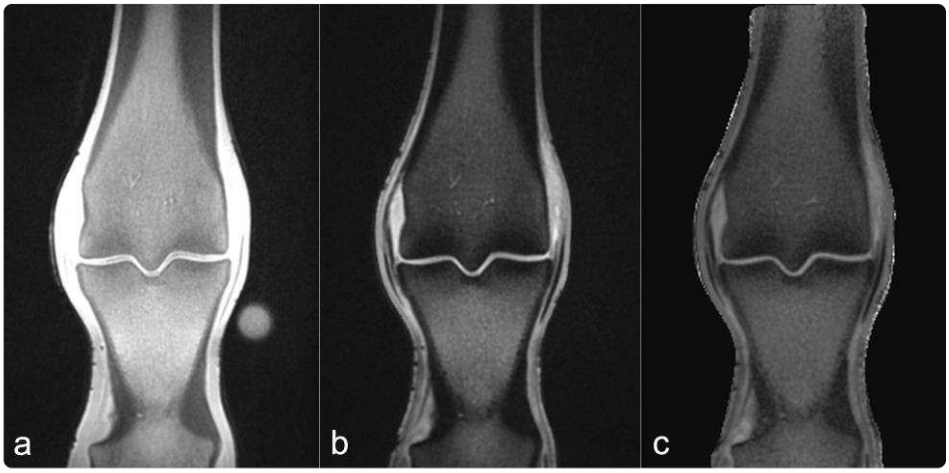


**Figure 1. Example MR images** UTE images were acquired using dual-echo UTE sequences. Image **(a)** was acquired with a short echo time of 0.04ms ($echo_1$). Image **(b)** was acquired with a longer echo time of 2.68ms ($echo_2$). For the PI image in panel **(c)** porosity index was calculated using the formula: $Porosity\ index\ (\%) = \frac{intensity\ echo_2}{intensity\ echo_1}\ x\ 100\%$. For presentation in this figure the background was manually set to zero.

To spatially align the CT and PI images, the PI image was registered to the CT image using Elastix software [36,37]. First, a manual rigid alignment was performed, followed by a multi-resolution affine registration using a mutual information metric. The resultant registered PI image matched the resolution of the CT image, allowing for voxel-to-voxel comparison.

The volume of the distal third metacarpal/ metatarsal bone was initially segmented from the QCT image following McPhee et al. (2023) [34], utilising ImageJ (NIH Image J 1.53 [35]). First, noise was removed by a median filter (kernel size = 2), before being converted to binary using a contrast-based local thresholding filter (kernel size = 50). Finally, the third metacarpal/ metatarsal bone was isolated from background voxels using a connectivity filter.

Co-registered images were loaded into an open-source 3D imaging software (Slicer [38]) and the diaphyseal part of segmentation of the third metacarpal/ metatarsal bone was manually removed to match the ROI to the distal condyle of the third metacarpal/ metatarsal bone.

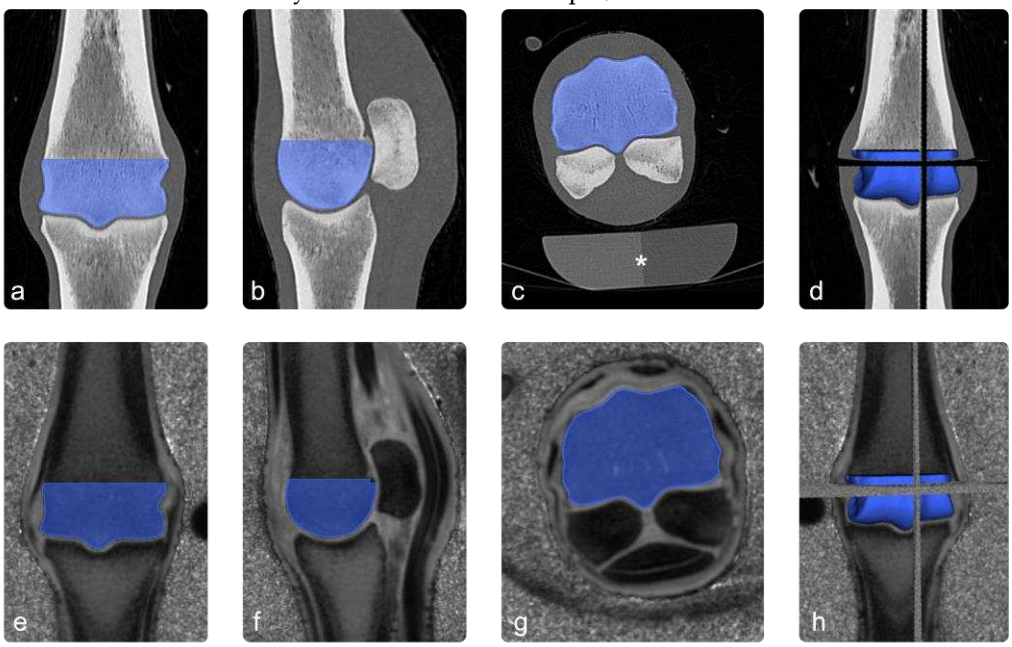


**Figure 2. Image processing**. Images **a, b and c** show the ROI (blue) in coronal, sagittal and transverse sections of the CT scan. In image **(d)** the 3 planes are combined to a 3D-ROI. The images **e to h** show

Preprints (www.preprints.org) | NOT PEER-REVIEWED | Posted: 7 August 2023 doi:10.20944/preprints202308.0477.v1



the co-registered PI images in the same way. The asterisk in image **(c)** highlights a standard osteodensitometry phantom containing calcium hydroxyapatite and demineralised water, which was used to calculate bone mineral density.

*Statistics*

Linear regression analysis was performed to determine the relationship between BMD and PI. Data was tested for normality using a Jarque-Bera test and subsequently a t-test was used to assess differences in r value between left and right limbs, forelimbs and hindlimbs as well as left and right forelimbs and left and right hindlimbs.

## 3. Results

### *3.1. Imaging*

All collected specimens underwent CT imaging. One forelimb was excluded from the study due to the presence of metallic surgical implants, which precluded its use for MR imaging and would have negatively impacted CT images as well as images processing. Therefore, eleven forelimbs and twelve hindlimbs were included in the final analysis.

### *3.2. Linear regression anlysis*

Linear regression analysis revealed a negative correlation between BMD and PI with a mean r-value of -0.29 (ranging from -0.14 to -0.43, SD: 0.071, SE: 0.014) and a mean slope of -0.0084 (ranging from -0.012 to -0.0048, SD: 0.0018, SE: 0.00038, example see Figure 3).

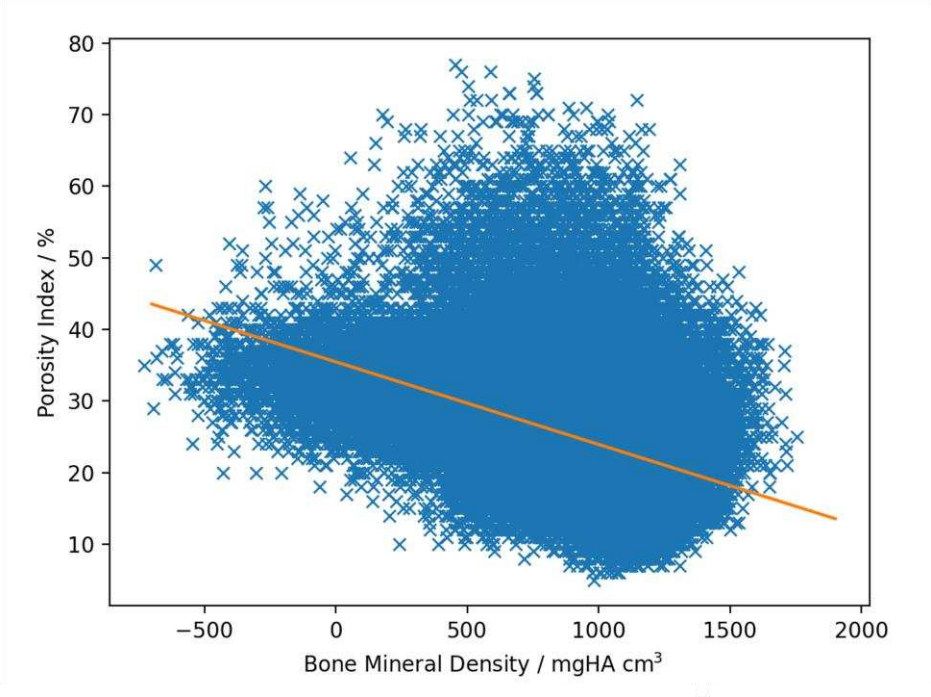


**Figure 3. Scatterplot example orf one specimen**. The volume of the distal third metacarpal/ metatarsal bone was initially segmented from the QCT image following McPhee et al. (2023) [34]. The whole metacarpal/ metatarsal condyle was included in the 3D-ROI. Care was taken to not include soft tissues surrounding the osseous structures. The same ROI was used in co-registered MR images. BMD values derived from CT images and PI images derived from MR images were plotted against each other for each pixel. The negative slope of -0.0087 indicates an inverse correlation between the two variables. The r-value of the plotted specimen was -0.43.

### *3.3. Inter limb comparison*

Preprints (www.preprints.org) | NOT PEER-REVIEWED | Posted: 7 August 2023 doi:10.20944/preprints202308.0477.v1



A stronger negative correlation between BMD and PI values was observed in the hindlimbs (mean r value: -0.26) when compared to forelimbs (mean r value: -0.32), which reached statistical significance (p=0.036). The remaining comparisons between left (mean r-value: -0.28) and right limbs (mean r value: -0.30), left forelimbs (mean r-value: -0.25) and right forelimbs (mean r value: -0.26) and left hind limbs (mean r value: -0.30) and right hindlimbs (mean r-value: -0.34) were not statistically significant with p-values of 0.39, 0.94 and 0.23 respectively. An overview of all obtained r-values can be seen in Table 1.

**Table 1.** Slope, standard error of the slope and r-value are listed per horse and per limb used in the study. The right forelimb of horse 1 was excluded due to the presence of metallic surgical implants. LF: left forelimb; RF: right forelimb: LH: left hindlimb; RH: right hindlimb.

| Specimen | Slope | Standard error of the slope | r value |
|---|---|---|---|
| Horse 1 LF | -0.012 | 9.13E-05 | -0.16 |
| Horse 1 RF | *excluded* | *excluded* | *excluded* |
| Horse 1 LH | -0.010 | 7.13E-05 | -0.23 |
| Horse 1 RH | -0.011 | 7.20E-05 | -0.24 |
| Horse 2 LF | -0.0098 | 6.87E-05 | -0.18 |
| Horse 2 RF | -0.0094 | 6.16E-05 | -0.29 |
| Horse 2 LH | -0.0094 | 5.83E-05 | -0.29 |
| Horse 2 RH | -0.0094 | 5.53E-05 | -0.35 |
| Horse 3 LF | -0.0090 | 6.87E-05 | -0.30 |
| Horse 3 RF | -0.0090 | 6.27E-05 | -0.34 |
| Horse 3 LH | -0.0094 | 5.41E-05 | -0.33 |
| Horse 3 RH | -0.0087 | 5.49E-05 | -0.43 |
| Horse 4 LF | -0.0086 | 5.89E-05 | -0.36 |
| Horse 4 RF | -0.0082 | 7.12E-05 | -0.29 |
| Horse 4 LH | -0.0084 | 5.70E-05 | -0.32 |
| Horse 4 RH | -0.0077 | 6.39E-05 | -0.30 |
| Horse 5 LF | -0.0074 | 8.36E-05 | -0.22 |
| Horse 5 RF | -0.0072 | 8.65E-05 | -0.24 |
| Horse 5 LH | -0.0074 | 7.14E-05 | -0.28 |
| Horse 5 RH | -0.0076 | 6.66E-05 | -0.30 |
| Horse 6 LF | -0.0069 | 7.25E-05 | -0.31 |
| Horse 6 RF | -0.0057 | 8.80E-05 | -0.14 |
| Horse 6 LH | -0.0048 | 7.27E-05 | -0.32 |
| Horse 6 RH | -0.0048 | 7.39E-05 | -0.40 |

## 4. Discussion

A negative correlation was found between BMD and PI in all limbs, hereby differences in r value between different groups were identified, reached statistical significance when comparing forelimbs to hindlimbs. While the clinical relevance and correlation to bone strength of this finding is currently unknown, it is in keeping with varying prevalence and severity of fatigue injury reported in the literature. Pinchbeck et al. (2013) state that POD is more pronounced in forelimbs, when compared to hindlimbs [3]. Similarly 72% of lateral condylar fractures occur in the forelimbs [2].

In addition to differences between fore- and hindlimb injury rates, discrepancies in injury occurrence have been reported for inside versus outside limbs, when taking race direction into account. The inside limb is affected in 47% of cases, however no significant association between race direction and laterality of the fractured limb was identified [2]. Racecourses in the UK are mixed and races are held in clockwise and counter-clockwise direction, additionally direction of training and

 doi:10.20944/preprints202308.0477.v1



training regime will have to be taken into consideration. No statistically significant difference was found between left and right limbs in this study.

A third variable described in the context of fatigue injury is the location of changes within the region of interest. While POD does more severely affect the medial condyle in forelimbs, the lateral condyle is the site of higher grade lesions in the hindlimbs [3]. Condylar fractures occur more frequently in parasagittal groove of the lateral condyle, when compared to medial [2,12]. The behavior of PI in these disease-prone regions would improve understanding of PI as a biomarker for bone strength. This could be of interest as a novel way to assess fracture risk in the equine athlete, as association between CT-derived BMD and injury could not be reliably established for condylar fractures in racehorses [22–24]. In human bones cortical PI has been shown to be a chief contributor of bone strength, which is related to fracture risk independent of BMD [39]. However, these studies are derived from human osteoporosis patients and their translational value is limited. Data on PI in the context of increased fracture risk in humans or horses has not been reported in the literature.

Most bones are divided into two components: cortical and trabecular bone. Trabecular bone absorbs shock and transfers mechanical loads to the cortical compartment. Cortical bone is the main contributor to bone strength [30,40,41]. The calculated numeral porosity value of the two compartments is not related. Cortical bone in human mandibular condyles shows an average porosity of 3.5% as compared to trabecular bone with an average porosity of 79.3% [42]. While these differences seem profound, the two components and their anatomical porosity have to be understood as a closely linked continuum, rather than completely separate from each other [40].

Cortical bone is the main component in the diaphysis of long bones. The equine distal McIII/MtIII condyle however represents the epiphysis and metaphysis of the bone and as such contains a much larger amount of trabecular bone, which cannot be ignored in assessment of condylar bone strength. Furthermore, trabecular bone in the equine condyle densifies in response to training and is replaced by compact bone, which is akin to cortical bone in density [24,43]. While recent human reports on porosity index and bone strength have focused on cortical porosity alone [30,32,44], considered assessment of the entire condyle as an anatomical and biomechanical unit is indicated. However, careful segmentation of cortical and trabecular bone could aid better understanding of the details of pathophysiological processes of fatigue injury in the equine athlete, as adaptive remodeling is different between cortical and trabecular bone [42]. Mechanical testing could shed light onto the relationship between PI of the combined trabecular and cortical components of the equine distal condyle and bone strength. Alternatively, the use of a limb specific finite element model, as developed by the group (S.MP. and U.W.) could be used to further investigations into condylar PI and bone strength [34].

The technical feasibility of MR-derived cortical porosity was demonstrated in human tibiae, which evaluated the technique against microCT measurements of pore size and porosity [32]. Hereby the use of UTE MRI and PI for bone imaging has several practical advantages. Firstly, studies can be carried out on a clinical MRI scanner with a standard knee coil. This allows scanning of intact, undissected specimens and assessment of the anatomical structures as a whole, rather than isolated, small samples as needed for other modalities such as microCT. Additionally, despite high field MRI scanners not being standard in large animal hospitals to this date, the availability of standard clinical equipment might still supersede availability of more specialized research equipment such as microCT or MRI of ultrahigh field strength. Besides the use of commercially available standard hardware, the software used in this study is also widely accessible. While a work-in-progress (WIP) dual-echo sequence was used for image acquisition in the current work, similar sequences are readily available on the market. The mathematics behind generating the PI images relies on a simple ratio between two images of different echo times and can therefore be computed with free open source image processing software and does not require specialized calibration against a phantom or the use of adiabatic inversion pulses as other markers utilized in quantitative MR bone imaging [29].

Besides the practical advantages of using standard clinical equipment, there are scientific benefits as well. The use of a 3T magnet is advantageous over ultrahigh field strength of research scanners, as the susceptibility artefact between water and bone is more pronounced with higher field

strengths, which impairs separation of BW and PW signal, making PI assessment more difficult [45]. Additionally, UTE MRI derived bone porosity measurements are an excellent indirect measure of bone microstructure, as it is capable of generating signal from all water protons within bones, including the ones located in micropores even beyond the resolution of microCT images [46].

## 5. Conclusions

UTE-MRI derived PI is a promising biomarker for assessment of bone health and strength. Better understanding of osseous porosity and its correlation with other biomarkers as well as disease patterns could improve our understanding of pathophysiological processes associated with fatigue injury and their presentation on clinical imaging modalities.

This proof-of-concept study was able to establish feasibility of the use of UTE-MRI in equine specimens and established an inverse correlation between BMD and condylar PI in the equine distal McIII/MtIII. Further work is needed to segment the equine condyle into its different osseous components and to evaluate PI in horses with and without clinically relevant stress injury of the metacarpal/ -tarsal condyle and correlate these patterns to training histories gathered with GPS data.

**Author Contributions:** Conceptualization, C.D., S.T., L.K.; methodology, C.D., S.T., S.MP., L.K., T.S.; software, C.D., S.MP., L.K., S.S.; formal analysis, C.D., L.K.; investigation, C.D., L.K.; resources, C.D., S.T., L.K., S.MP.; data curation, C.D., S.MP., L.K.; writing—original draft preparation, C.D.; writing—review and editing, C.D., S.T., S.MP., U.W., T.S., S.S., L.K.; visualization, C.D.; supervision, S.T., L.K., U.W.; project administration, C.D., L.K.; funding acquisition, C.D., S.T., L.K. All authors have read and agreed to the published version of the manuscript.

**Funding:** This work was part funded by Siemens Healthcare Limited (IPA 42) and part funded by the Horseracing Betting Levy Board. Lucy Kershaw is funded by GlaxoSmithKline.

**Institutional Review Board Statement:** The animal study protocol was approved by the Veterinary Ethical Review Committee (VERC) of the Royal (Dick) School of Veterinary Studies and The Roslin Institute, The University of Edinburgh, Edinburgh (VERC reference: 165.22).

**Informed Consent Statement:** Informed consent was obtained for all cases used in the study.

**Acknowledgments:** We would like to thank Chandra Logie and Craig Pennycook for their help with sample collection. Furthermore, we are grateful to the owners for donating their horses.

**Conflicts of Interest:** S.S. is employed by Siemens Healthineers. The funders had no role in the design of the study; in the collection, analyses, or interpretation of data; in the writing of the manuscript; or in the decision to publish the results.

## References

1. Barr, E., et al., *Post mortem evaluation of palmar osteochondral disease (traumatic osteochondrosis) of the metacarpo/metatarsophalangeal joint in Thoroughbred racehorses.* Equine veterinary journal, 2009. **41**(4): p. 366-371.
2. Parkin, T., et al., *Catastrophic fracture of the lateral condyle of the third metacarpus/metatarsus in UK racehorses–fracture descriptions and pre-existing pathology.* The Veterinary Journal, 2006. **171**(1): p. 157-165.
3. Pinchbeck, G., et al., *Pathological and clinical features associated with palmar/plantar osteochondral disease of the metacarpo/metatarsophalangeal joint in T horoughbred racehorses.* Equine veterinary journal, 2013. **45**(5): p. 587-592.
4. Pinchbeck, G., et al., *Horse-, training-and race-level risk factors for palmar/plantar osteochondral disease in the racing T horoughbred.* Equine veterinary journal, 2013. **45**(5): p. 582-586.
5. Ross, M.W. and S.J. Dyson, *Diagnosis and Management of Lameness in the Horse*. 2010: Elsevier Health Sciences.
6. Davis, A., et al., *Improved radiological diagnosis of palmar osteochondral disease in the Thoroughbred racehorse.* Equine veterinary journal, 2017. **49**(4): p. 454-460.
7. Sherlock, C.E., T.S. Mair, and F. Ter Braake, *Osseous lesions in the metacarpo (tarso) phalangeal joint diagnosed using low-field magnetic resonance imaging in standing horses.* Veterinary Radiology & Ultrasound, 2009. **50**(1): p. 13-20.
8. Murray, R.C., et al., *Validation of magnetic resonance imaging for measurement of equine articular cartilage and subchondral bone thickness.* American journal of veterinary research, 2005. **66**(11): p. 1999-2005.
9. Riggs, C., G. Whitehouse, and A. Boyde, *Pathology of the distal condyles of the third metacarpal and third metatarsal bones of the horse.* Equine veterinary journal, 1999. **31**(2): p. 140-148.

10. Muir, P., et al., *Exercise-induced metacarpophalangeal joint adaptation in the Thoroughbred racehorse.* Journal of anatomy, 2008. **213**(6): p. 706-717.
11. Allen, S., et al., *Description of veterinary events and risk factors for fatality in National Hunt flat racing Thoroughbreds in Great Britain (2000–2013).* Equine veterinary journal, 2017. **49**(6): p. 700-705.
12. Parkin, T., et al., *Risk of fatal distal limb fractures among thoroughbreds involved in the five tpes of racing in the United Kingdom.* Veterinary Record, 2004. **154**(16): p. 493-497.
13. Zekas, L.J., et al., *Characterisation of the type and location of fractures of the third metacarpal/metatarsal condyles in 135 horses in central Kentucky (1986–1994).* Equine veterinary journal, 1999. **31**(4): p. 304-308.
14. Datir, A., et al., *Stress-related bone injuries with emphasis on MRI.* Clinical radiology, 2007. **62**(9): p. 828-836.
15. Wentz, L., et al., *Females have a greater incidence of stress fractures than males in both military and athletic populations: a systemic review.* Military medicine, 2011. **176**(4): p. 420-430.
16. Whitton, R., et al., *Subchondral bone microdamage accumulation in distal metacarpus of Thoroughbred racehorses.* Equine veterinary journal, 2018. **50**(6): p. 766-773.
17. Gupta, H. and P. Zioupos, *Fracture of bone tissue: the 'hows' and the 'whys'.* Medical engineering & physics, 2008. **30**(10): p. 1209-1226.
18. Verheyen, K., et al., *Exercise distance and speed affect the risk of fracture in racehorses.* Bone, 2006. **39**(6): p. 1322-1330.
19. Chapurlat, R. and P. Delmas, *Bone microdamage: a clinical perspective.* Osteoporosis international, 2009. **20**: p. 1299-1308.
20. Bates, D.W., D.M. Black, and S.R. Cummings, *Clinical use of bone densitometry: clinical applications.* Jama, 2002. **288**(15): p. 1898-1900.
21. Adams, A.L., et al., *Osteoporosis and hip fracture risk from routine computed tomography scans: the fracture, osteoporosis, and CT utilization study (FOCUS).* Journal of Bone and Mineral Research, 2018. **33**(7): p. 1291-1301.
22. Bogers, S.H., et al., *Quantitative comparison of bone mineral density characteristics of the distal epiphysis of third metacarpal bones from Thoroughbred racehorses with or without condylar fracture.* American journal of veterinary research, 2016. **77**(1): p. 32-38.
23. Firth, E.C., et al., *The effect of previous conditioning exercise on diaphyseal and metaphyseal bone to imposition and withdrawal of training in young Thoroughbred horses.* The Veterinary Journal, 2012. **192**(1): p. 34-40.
24. Loughridge, A., et al., *Qualitative assessment of bone density at the distal articulating surface of the third metacarpal in Thoroughbred racehorses with and without condylar fracture.* Equine veterinary journal, 2017. **49**(2): p. 172-177.
25. Iori, G., et al., *Large cortical bone pores in the tibia are associated with proximal femur strength.* PLoS One, 2019. **14**(4): p. e0215405.
26. Musy, S.N., et al., *Not only stiffness, but also yield strength of the trabecular structure determined by non-linear μFE is best predicted by bone volume fraction and fabric tensor.* Journal of the mechanical behavior of biomedical materials, 2017. **65**: p. 808-813.
27. Zebaze, R., et al., *Increased cortical porosity and reduced trabecular density are not necessarily synonymous with bone loss and microstructural deterioration.* JBMR plus, 2019. **3**(4): p. e10078.
28. Kral, R., et al., *Women with fracture, unidentified by FRAX, but identified by cortical porosity, have a set of characteristics that contribute to their increased fracture risk beyond high FRAX score and high cortical porosity.* Bone, 2018. **116**: p. 259-265.
29. Ma, Y.-J., et al., *Quantitative ultrashort echo time (UTE) magnetic resonance imaging of bone: an update.* Frontiers in Endocrinology, 2020. **11**: p. 667.
30. Jones, B.C., et al., *MRI-derived porosity index is associated with whole-bone stiffness and mineral density in human cadaveric femora.* Bone, 2021. **143**: p. 115774.
31. Manhard, M.K., et al., *MRI-derived bound and pore water concentrations as predictors of fracture resistance.* Bone, 2016. **87**: p. 1-10.
32. Rajapakse, C.S., et al., *Volumetric cortical bone porosity assessment with MR imaging: validation and clinical feasibility.* Radiology, 2015. **276**(2): p. 526-535.
33. Chang, E.Y., et al., *Ultrashort echo time magnetization transfer (UTE-MT) imaging of cortical bone.* NMR in Biomedicine, 2015. **28**(7): p. 873-880.
34. McPhee, S., et al., *QCT-based computational bone strength assessment updated with MRI derived'hidden'microporosity.* bioRxiv, 2023: p. 2023.03. 30.534902.
35. Abràmoff, M.D., P.J. Magalhães, and S.J. Ram, *Image processing with ImageJ.* Biophotonics international, 2004. **11**(7): p. 36-42.
36. Klein, S., et al., *Elastix: a toolbox for intensity-based medical image registration.* IEEE transactions on medical imaging, 2009. **29**(1): p. 196-205.
37. Shamonin, D.P., et al., *Fast parallel image registration on CPU and GPU for diagnostic classification of Alzheimer's disease.* Frontiers in neuroinformatics, 2014. **7**: p. 50.

38. Fedorov, A., et al., *3D Slicer as an image computing platform for the Quantitative Imaging Network.* Magnetic resonance imaging, 2012. **30**(9): p. 1323-1341.
39. Bjørnerem, Å., *The clinical contribution of cortical porosity to fragility fractures.* BoneKEy reports, 2016. **5**.
40. Cooper, D., et al., *Cortical bone porosity: what is it, why is it important, and how can we detect it?* Current osteoporosis reports, 2016. **14**: p. 187-198.
41. Ott, S.M., *Cortical or trabecular bone: what's the difference?* American journal of nephrology, 2018. **47**(6): p. 373-375.
42. Renders, G., et al., *Porosity of human mandibular condylar bone.* Journal of anatomy, 2007. **210**(3): p. 239-248.
43. Liley, H., et al., *Statistical modeling of the equine third metacarpal bone incorporating morphology and bone mineral density.* Plos one, 2018. **13**(6): p. e0194406.
44. Chen, M. and H. Yuan, *Assessment of porosity index of the femoral neck and tibia by 3D ultra-short echo-time MRI.* Journal of Magnetic Resonance Imaging, 2018. **47**(3): p. 820-828.
45. Seifert, A.C. and F.W. Wehrli, *Solid-state quantitative 1 H and 31 P MRI of cortical bone in humans.* Current osteoporosis reports, 2016. **14**: p. 77-86.
46. Jerban, S., et al., *Ultrashort echo time magnetic resonance imaging (UTE-MRI) of cortical bone correlates well with histomorphometric assessment of bone microstructure.* Bone, 2019. **123**: p. 8-17.